Structure of Hjc, a Holliday junction resolvase, from *Sulfolobus solfataricus*

Charles S. Bond*†, Mamuka Kvaratskhelia‡§, Derek Richard‡, Malcolm F. White‡, and William N. Hunter*

*Wellcome Trust Biocentre, University of Dundee, Dundee, Tayside DD1 5EH, United Kingdom; and ‡Centre for Biomolecular Science, University of St. Andrews, St. Andrews, Fife KY16 9ST, United Kingdom

Edited by Kiyoshi Mizuuchi, National Institutes of Health, Bethesda, MD, and approved March 9, 2001 (received for review December 22, 2000)

The 2.15-Å structure of Hjc, a Holliday junction-resolving enzyme from the archaeon *Sulfolobus solfataricus*, reveals extensive structural homology with a superfamily of nucleases that includes type II restriction enzymes. Hjc is a dimer with a large DNA-binding surface consisting of numerous basic residues surrounding the metal-binding residues of the active sites. Residues critical for catalysis, identified on the basis of sequence comparisons and site-directed mutagenesis studies, are clustered to produce two active sites in the dimer, about 29 Å apart, consistent with the requirement for the introduction of paired nicks in opposing strands of the four-way DNA junction substrate. Hjc displays similarity to the restriction endonucleases in the way its specific DNA-cutting pattern is determined but uses a different arrangement of nuclease subunits. Further structural similarity to a broad group of metal/phosphate-binding proteins, including conservation of active-site location, is observed. A high degree of conservation of surface electrostatic character is observed between Hjc and T4-phage endonuclease VII despite a complete lack of structural homology. A model of the Hjc–Holliday junction complex is proposed, based on the available functional and structural data.

The repair and rearrangement of DNA by homologous recombination generates Holliday junctions (four-way DNA junctions) that create a physical link between homologous duplex DNA molecules. Holliday junctions are mobile entities that branch-migrate through the linked DNA molecules, in the process generating segments of heteroduplex DNA caused by mutual-strand exchange (reviewed in refs. 1 and 2). Unresolved Holliday junctions are themselves potent mutagens if allowed to persist through to the point where DNA is replicated. It is therefore vital to resolve junctions, and normally this is accomplished by the introduction of paired nicks in the phosphodiester backbone on opposing strands of the junction, releasing heteroduplex DNA products. This reaction is catalyzed by a class of structure-specific endonucleases known as the Holliday junction-resolving enzymes. Because homologous recombination is a ubiquitous process, it is perhaps not surprising that junction-resolving enzymes are known in eubacteria and their phage, fungal mitochondria, eukaryotic pox viruses, and more recently, the archaea (reviewed in ref. 3). However, despite extensive searches using both biochemical and genetic techniques, a eukaryotic nuclear Holliday junction-resolving enzyme remains elusive.

The study of junction-resolving enzymes has progressed over recent years by means of a wide variety of enzymological, spectroscopic, molecular biological, and structure–function studies (reviewed in ref. 4). The three x-ray structures published [*Escherichia coli* RuvC (5), bacteriophage T4 endonuclease VII (6), and phage T7 endonuclease I (7)] show three unrelated protein folds, emphasizing the diversity of this class of enzymes. Although all of the junction-resolving enzymes catalyze the hydrolysis of the phosphodiester backbone by utilizing a metal-activated hydroxyl ion, they differ significantly in their means of recognition and manipulation of the four-way DNA junction substrate. Our understanding of the recognition step for any of these enzymes still remains limited, and structures of DNA·protein complexes have remained elusive to date.

The archaea are now recognized to constitute a third domain of Life, distinct from both the eukarya and eubacteria (8). Archaea possess striking similarities to the eukarya in their information-processing pathways, including DNA replication, repair, and transcription, and for this reason they have become the focus of increasing attention. The archaeal Holliday junction-resolving enzyme, Hjc, was identified recently in *Pyrococcus furiosus* (9) and *Sulfolobus solfataricus* (10). Extensive manipulation of both the global and local structure of the Holliday junction by *Sulfolobus* Hjc has been demonstrated by chemical probing and comparative gel electrophoresis (11). Hjc has a conserved sequence motif $[E(X)_nPD(X)_mEXK]$ previously identified in a wide range of nucleases, where it constitutes the catalytic metal ion-binding domain (reviewed in ref. 12). This feature has allowed the N-terminal half of Hjc to be modeled by using the catalytic domain of the type II restriction enzyme *Eco*RV (11).

We report here the crystal structure of *Sulfolobus* Hjc, determined by using multiple-wavelength anomalous dispersion, to a resolution of 2.15 Å.

Experimental Procedures

Sample Preparation. Native Hjc was cloned, expressed, and purified as described (11). To incorporate selenium, the methionine auxotrophic strain of *E. coli*, B834(DE3), was heat-shock transformed with the plasmid carrying the gene for *S. solfataricus* Hjc with a substitution R13M (M.F.W., unpublished data), and selected on Luria–Bertani agar plates containing 100 $mg \cdot ml^{-1}$ ampicillin. The mutant was used to include a second methionine in addition to Met-56. Bacteria were cultured in M9 medium supplemented with the usual amino acids except L-selenomethionine (100 $mg \cdot liter^{-1}$), which replaced L-methionine. Matrix-assisted laser desorption ionization time-of-flight mass spectrometry (PerSeptive Biosystems, Framingham, MA) was used to assess selenium incorporation. Hexagonal crystals appear in 20% (wt/vol) polyethylene glycol 4000/0.08 M sodium acetate (pH 4.6)/160 mM ammonium sulfate/20% glycerol within 2 weeks. Serial seeding into fresh crystallization medium in sitting drop plates (10-μl drop size) allows production of needles of dimensions $1 \times 0.05 \times 0.05$ mm^3. Microseeding into selenomethionine derivative-containing drops followed by macroseeding into fresh drops allowed production of diffraction-quality crystals of the selenomethionine derivative.

This paper was submitted directly (Track II) to the PNAS office.

Data deposition: The atomic coordinates and structure factors have been deposited in the Protein Data Bank, www.rcsb.org (PDB ID code 1HH1).

†To whom reprint requests should be addressed. E-mail: C.S.Bond@dundee.ac.uk.

§Present address: National Cancer Institute, Frederick, MD 21702.

The publication costs of this article were defrayed in part by page charge payment. This article must therefore be hereby marked "*advertisement*" in accordance with 18 U.S.C. §1734 solely to indicate this fact.

Table 1. Experimental details

	Native	Selenomethionine derivative		
Data				
Space group			$P6_122$	
Cell constants, Å	$a = 52.70$		$a = 52.85$	
	$c = 207.61$		$c = 208.30$	
Wavelength, Å	0.97626	0.97931	0.97961	0.93928
Resolution, Å	20.0–2.15	20.0–2.40	20.0–2.40	20.0–2.20
Observations	121,253	77,229	61,733	100,170
Unique reflections	10,061	7,441	7,308	9,460
R_{sym}*	0.041 (0.105)	0.036 (0.095)	0.041 (0.112)	0.042 (0.125)
R_{anom}*		0.029 (0.064)	0.033 (0.085)	0.030 (0.117)
Completeness, %*	99.2 (97.0)	99.2 (96.3)†	94.7 (90.2)†	94.8 (68.7)†
$\langle I \rangle / \langle \sigma I \rangle$*	36 (7.5)	13.6 (3.6)	13.1 (3.2)	9.9 (4.2)
Wilson B, Å^2	25	27	27	28
FOM (SOLVE)			0.34	
FOM (RESOLVE)			0.64	
Refinement				
R factor	0.220	Ramachandran outliers, %		3.6
R free (5%)	0.281	Cruickshank's DPI		0.217
No. of atoms	1,077	Average *B* factor, Å^2		35
Protein	998	Protein		34
Waters	79	Waters		39

FOM, Figure of merit. DPI, diffraction-component precision index.
*Figures in parentheses represent the highest resolution shell.
†Friedel pairs treated as separate.

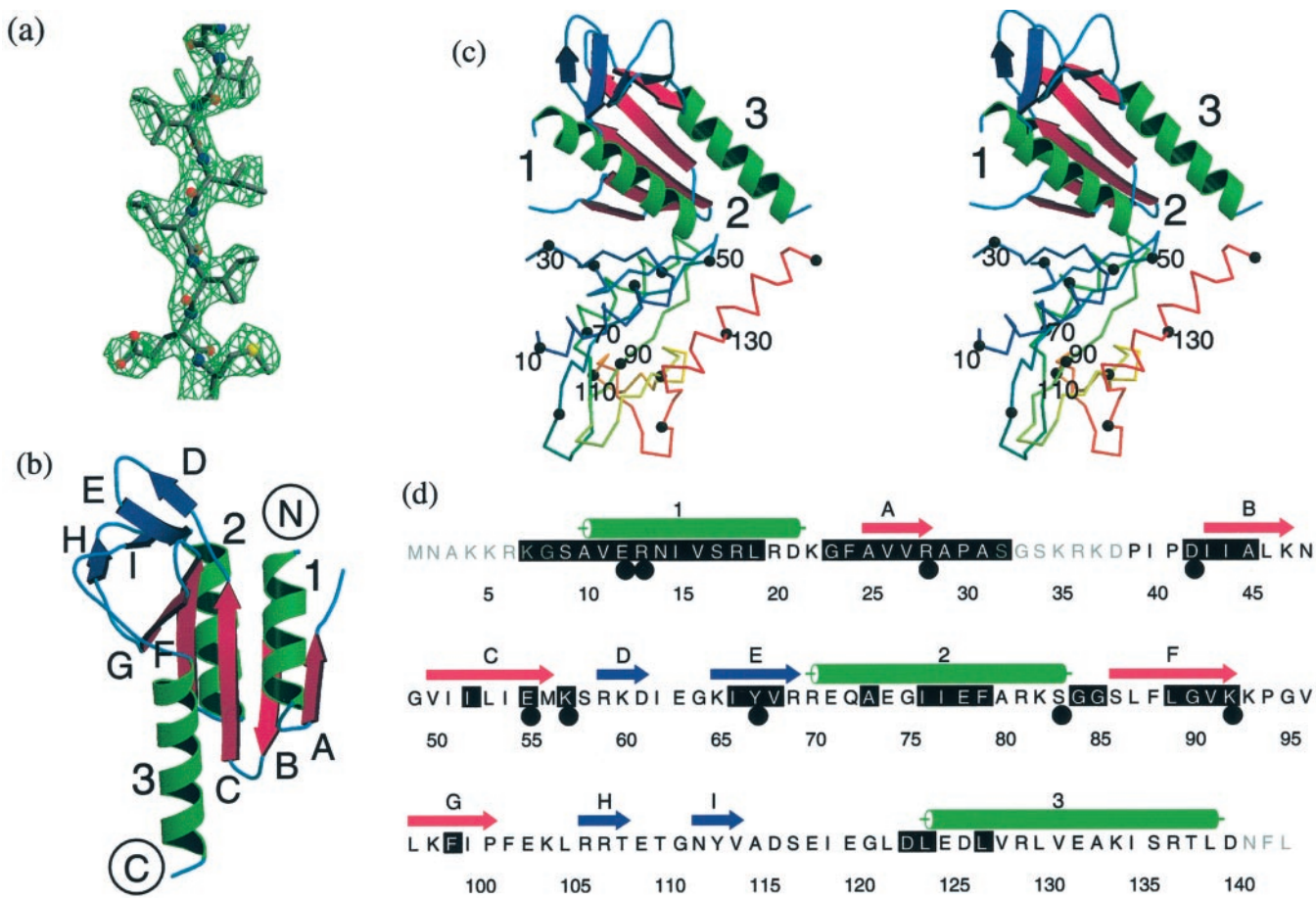

Fig. 1. The structure of *S. solfataricus* Hjc. (*a*) Solvent-flattened experimental electron density (1.3σ) for residues in strand C superimposed on the final model. (*b*) Ribbon representation of the Hjc monomer. The core β-sheet is shown as magenta arrows, α-helices are shown as green ribbon, and the peripheral β-sheet is shown as blue arrows. (*c*) Stereo representation of the Hjc dimer. One subunit is colored as above, with helices 1–3 labeled. The second subunit is a trace colored from blue at the N terminus to red at the C terminus. Every tenth C^{α} atom is marked by a black sphere and every twentieth is labeled. (*d*) The amino acid sequence of Hjc. Secondary structure elements are colored as above. Black shading marks residues that are highly conserved among Hjc family members. Large black circles mark residues for which mutation is deleterious to function. *a*–*d* were prepared by using MOLSCRIPT (36), RASTER3D (37), and ALSCRIPT (38). Secondary structure was assigned by using DSSP (39).

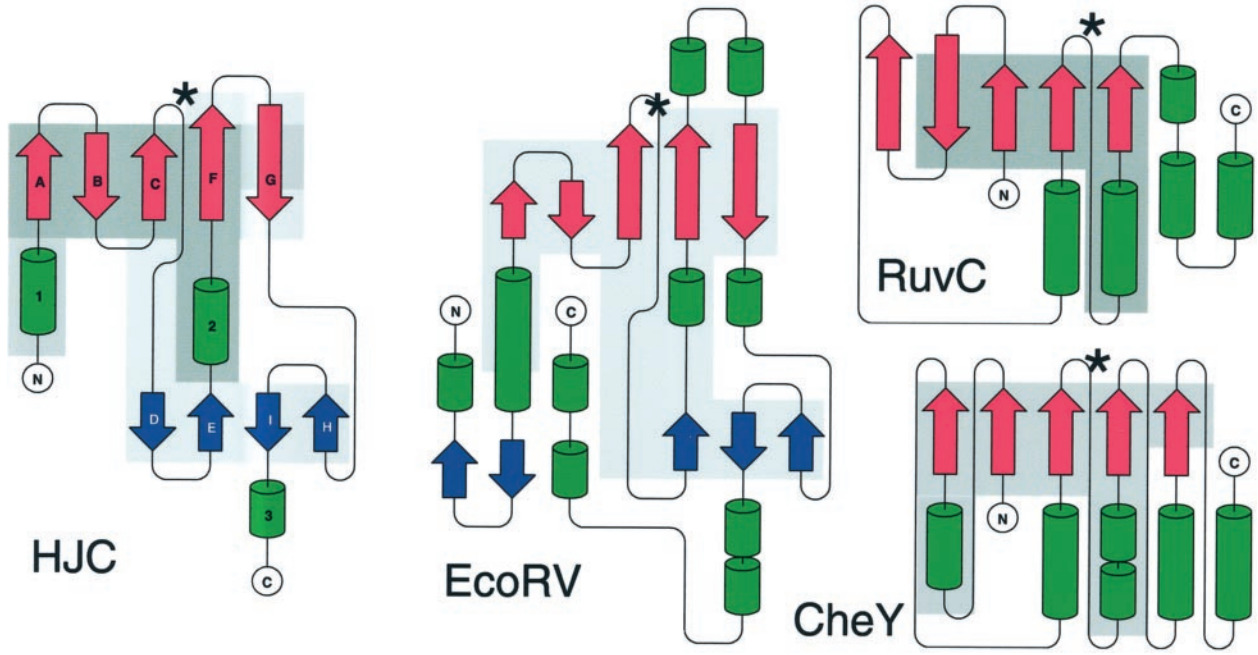

Fig. 2. The topologies of Hjc, *Eco*RV, *Thermotoga maritima* CheY, and *E. coli* RuvC. Asterisks mark the position of the divalent metal-binding site of each enzyme. Shading marks regions where Hjc shows structural similarity to the other enzymes. Prepared by using PROMOTIF (40) and TOPDRAW (available from authors).

Data Collection and Structure Solution. Details are given in Table 1. Native data to 2.15 Å were collected, on a hexagonal crystal cryocooled to 100 K directly from the drop, at the European Synchrotron Radiation Facility (Grenoble, France) BM14 (MAR CCD). The crystals clearly diffract beyond 2.15 Å, but the long *c* axis of over 200 Å enforced this limit to minimize diffraction spot overlap. There is one molecule of Hjc per asymmetric unit, corresponding to a solvent content of *ca.* 53%. A three-wavelength (f″ peak, inflection point ,and high-energy remote) anomalous dispersion experiment was carried out to 2.2-Å resolution, on a single cryocooled R13M mutant crystal of the selenomethionine derivative, at the European Synchrotron Radiation Facility BM14. All data were processed and scaled with DENZO and SCALEPACK (13) and phasing was performed with SOLVE (14), followed by solvent-flattening with RESOLVE (15). One well ordered and one disordered selenium site were found, which were later shown to be consistent with selenomethionine residues at positions 56 and 13. The phasing process yielded an interpretable electron map in space group $P6_122$ (Fig. 1*a*). The structure of the selenomethionine derivative was built by using WARP (16) (70% of the complete model) and O (17) and refined against all data (10,061 reflexions) by using REFMAC [atomic positions and isotropic thermal parameters using bulk solvent correction and a maximum-likelihood target (18)]. Progress of refinement was monitored throughout by the use of R_{free} (19) (5% of data), PROCHECK (20), and WHATCHECK (21). This model then was refined and rebuilt similarly with the native data. Water molecules were added where suitable electron-density features and hydrogen-bonding partners were evident.

Results and Discussion

The final model of native Hjc contains residues 9–31 and 39–140, with residues absent because of disorder at the termini (1–8 and 141–143) and at positions 32–38. Two residues, Y67 and R81, clearly show dual side-chain conformations and have been modeled as such. Residues 57–59 and 91–95 are in poorly defined electron density, resulting in elevated temperature factors and three residues in "generously allowed" regions of a Ramachandran plot. Two water molecules close to symmetry axes are modeled with half-occupancy. Further details are presented in Table 1.

Hjc is a compact α/β protein (Fig. 1) with a five-stranded mixed β-sheet at its core (strands A-B-C-F-G), flanked by two α-helices on one side (helices 1 and 3) and one α-helix (helix 2) on the other, and an additional four-stranded, antiparallel β-sheet (strands D-E-I-H). The functional Hjc homodimer is formed by a crystallographic two-fold axis (Fig. 1*c*; symmetry operation $x, -y, -z$ in orthogonal space). Residues involved in this interaction belong to the hydrophobic face of the β-sheets of each subunit.

The catalytic site of Hjc is identified by a cluster of conserved acidic residues that are proposed to bind the essential Mg^{2+} ions, based on predicted homology to the type II restriction endonucleases (11). No metal ions are present in this structure. The association of the monomers presents both active sites on one flat face of the dimer (the left-hand side in Fig. 1*c*), separated by a distance of about 29 Å. The dimer forms an "S" shape when viewed facing the active sites with metal-binding sites enclosed in the loops of the "S" (see *Surface Characteristics*).

Structural Homology. Proteins with folds similar to that of Hjc [DALI (22)] compose two broad groups. Comparison with the nucleases (type II restriction enzymes, λ-exonuclease, etc.) supports the recent predictions (11, 23) of the membership of Hjc in this family. A lower level of similarity is found with a group including tRNA synthetases and chemotaxis proteins.

The topology of the Hjc monomer is effectively a subset of that of the type II restriction enzymes, represented by *Eco*RV in Fig. 2, with all the secondary structure elements of Hjc except helix 3 having structural equivalents in *Eco*RV. A number of residues, which are known from biochemical analysis to be involved in catalysis in *Eco*RV (24, 25) and Hjc (refs. 11, 26, 27; Fig. 1*d*), occur in equivalent positions. More specifically, least-squares superposition (LSQMAN, ref. 28) of C^{α} atoms of Hjc and *Eco*RV [Protein Data Bank code 1RVA (29)] yield an rms difference of 2.1 Å over 72 structurally similar residues, representing over half of the Hjc polypeptide. Many functionally important residues are among the 12 substitutions to similar residue types and 10

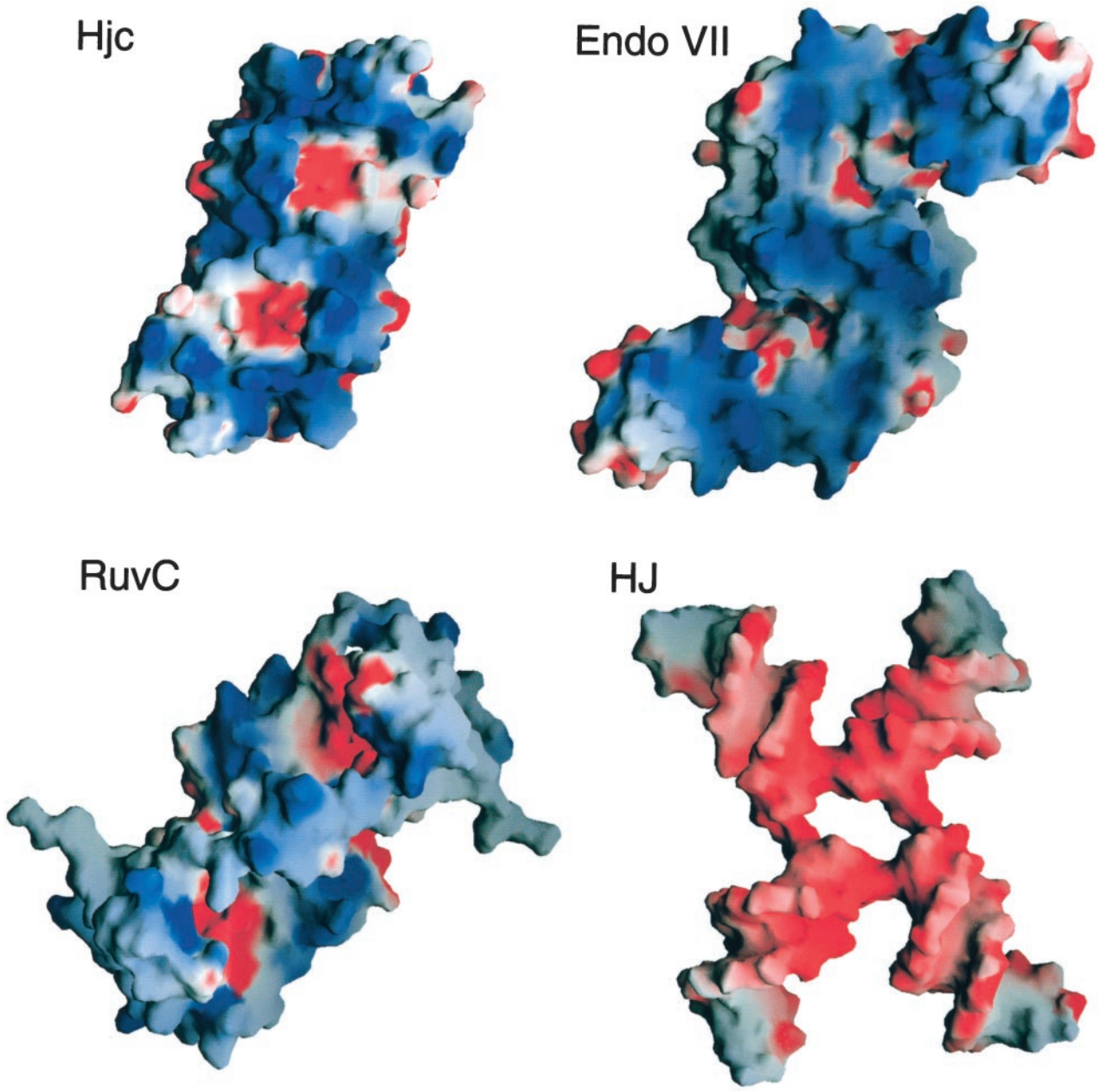

Fig. 3. The DNA-binding surfaces of Hjc, T4 endonuclease VII, and RuvC colored by electrostatic potential (blue represents positive and red represents negative charge). For comparison, the surface of a Holliday junction (HJ) computer-modeled in the X-shaped global structure predicted for junction bound by Hjc also is shown. Prepared by using GRASP (41).

identical aligned residues. Similar comparisons with other type II restriction enzymes [*Mun*I (30) and *Pvu*II (31); not shown] suggest that the intact Hjc subunit represents a minimal nuclease domain lacking the longer loops present in restriction enzymes. This observation is consistent with Hjc being a protein from a hyperthermophile and its concomitant requirement for high stability.

A striking structural homology was noted with the bacterial chemotaxis protein CheY from *Thermotoga maritima* [Protein Data Bank code 1TMY (32)]. Fig. 2 depicts the high level of similarity between Hjc and CheY, but even though the β-sheets clearly have different topologies with strands B and D running in opposite directions, the overall effect on structure is minimal, with side chains occupying similar positions. Superposition of Hjc and CheY yields an rms difference of 2.3 Å for 56 C^{α} atoms, which extends to 2.3 Å for 65 C^{α} atoms if the order in sequence and chain direction is ignored. CheY, a signal transduction protein, is unrelated functionally to the nucleases, yet its requirement for catalytic Mg^{2+} and binding of phosphate provide an explanation for structural similarity, as the relevant amino acids are found in the same location (marked with an asterisk in Fig. 2). It is notable that *T. maritima* CheY, being like Hjc from a thermophile, also has short loops connecting its secondary structure elements.

Catalytic and DNA-Binding Residues. The conserved catalytic and metal-binding residues have been well characterized in *Eco*RV (24, 25). In Hjc, residues Glu-12, Pro-41, Asp-42, Glu-55, and Lys-57 are equivalent to Glu-45, Pro-73, Asp-74, Asp-90, and Lys-92 in *Eco*RV and their mutation leads to inactivation of the

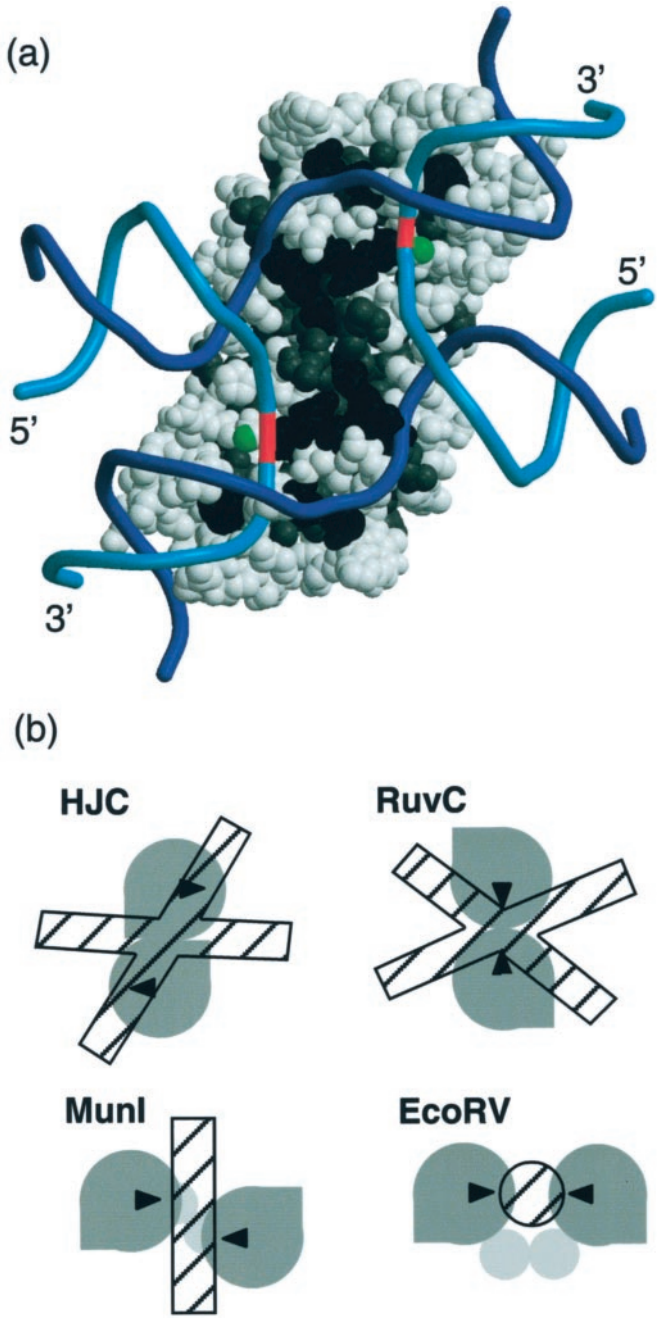

Fig. 4. (*a*) A model of Holliday junction DNA bound to Hjc. Hjc is shown as Corey–Pauling–Koltun spheres with residues conserved among Hjc sequences (gray) and residues for which mutants are inactive (black). A green ball marks the proposed metal-binding site. DNA is shown as a phosphate-backbone trace (exchange strand, cyan; continuous strand, blue), with the cleavage point highlighted in red. Prepared by using MOLSCRIPT (36). (*b*) Varying arrangements of similar nuclease domains produce different DNA-nicking patterns for the resolving enzymes Hjc and RuvC and the endonucleases *Eco*RV and *Mun*I. Gray shapes indicate nuclease domains, with black triangles at the nicking site. DNA is represented by hatched rectangles or a circle.

enzyme (11). Poor electron density for Lys-57, Ser-58, and Arg-59 and a difference in backbone conformation in comparison with the *Eco*RV–DNA complex (29) suggest that reordering of this span takes place on metal- and/or DNA-binding. Most of the residues for which mutants in *P. furiosus* Hjc (26) have been shown to impair function (Fig. 1*d*) are the metal-binding residues mentioned above, hydrophobic residues involved in dimerization (Phe-24 and Phe-79), or basic residues proposed to interact with DNA (Arg-13, Arg-28, and Lys-92). A common feature of the disordered regions (1–9, 32–38, and 90–95) is the presence of two or more consecutive arginine or lysine residues flanked on one or both sides by flexible residues such as glycine and serine (see Fig. 1*d*). We propose that these short loops are involved also in recognizing and binding DNA and are likely to adopt rigid conformations only on interaction with DNA.

Oligomerization. The active dimer is formed mainly by the interaction of hydrophobic residues on one face of the N-terminal portion of the main β-sheet. The surface area buried per monomer on dimerization is 737 Å^2 provided by the interaction of 39 pairs of atoms [AREAIMOL (18)]. There is a second, weaker interaction between pairs of dimers that also has some hydrophobic character. It is formed by the loops between strands D and E and I and H in the peripheral β-sheet, which interlock, burying 511 Å^2 per monomer from 21 pairs of atoms. *In vitro*, Hjc has been shown to form higher oligomers that render the enzyme inactive (M.K., B. N. Wardleworth, and M.F.W., unpublished observations), and it may be this second interaction that is responsible.

Surface Characteristics. The surface of Hjc responsible for binding to DNA is conspicuously basic (Fig. 3), even with the seven basic residues at positions 4–7 and 35–37 absent from the model. An "S" shape of positive charge formed around the molecular dyad snakes around the metal-binding sites. The profile of the surface is flat, although the structure of the polypeptide preceding and following the loop from positions 32–38 suggests that these residues will protrude out at the center of the dyad. Proline residues at either end of the loop may enforce this arrangement. This protuberance at the center of the junction is reminiscent of the acidic pins observed in RuvA (33), suggesting a possible role in stabilizing the disrupted junction center during catalysis.

Holliday Junction Binding. Hjc manipulates the junction into an "X" shape with acute angles of about 60°, and the strand that exchanges through this acute angle is cut three bases 3′ of the point of exchange (11). On the arm containing the cleavage site, base pair disruption occurs up to at least four base pairs after the point of exchange, whereas minimal disruption of the other arm is seen (11). The similarity of the catalytic site to the type II restriction endonucleases limits the arrangement of the arm containing the cleavage site. These various factors place a number of constraints on the modes of binding that have been taken into account in the model proposed in Fig. 4*a*. In this model, the exchanging strand is in close contact with the protein only at the point of cleavage. The helix disruption at the junction center leads to the separated continuous strand passing around the catalytic site and interacting with a patch of conserved residues around Lys-92, Arg-13, and Arg-28 before pairing with the other exchanging strand. The effects of residues at the N terminus and positions 32–38 on this model cannot be foreseen, but it should be noted that their approximate positions suggest interactions with the unpaired section of the continuous strand.

Functional Homologs. Crystal structures for three other junction-resolving enzymes [*E. coli* RuvC (5), T4 phage endonuclease VII (6) and T7 phage endonuclease I (7)] are known. These enzymes share no sequence homology but all are active as dimers. Initial comparisons with endonuclease I show that despite having a related nuclease superfamily fold, it has a different mode of dimerization involving swapping of one β-strand and α-helix between monomers via an extended linker (not shown). Endonuclease VII has a fold that involves extensive swapping of secondary structure elements between subunits and a structural zinc ion, and bears no resemblance whatsoever to Hjc, yet

inspection of the two enzymes' surface electrostatic characters shows a high degree of similarity (Fig. 3). As with Hjc, the distribution of basic residues around the dyad in endonuclease VII produces an "S" shape with catalytic metal-binding residues providing acidic patches, although the DNA-binding face is slightly concave rather than flat in profile. The other faces of Hjc and endonuclease VII (not shown) bear little similarity and have no distinguishing features. The endonuclease VII dimer has a volume of 41,997 $Å^3$ compared with the more compact 32,770 $Å^3$ of Hjc. A contribution to this volume difference comes from additional lobes at the end of the "S" of endonuclease VII. Examination of the DNA-binding mode of *Eco*RV suggests this region is involved in DNA binding in Hjc, and is shown as such in Fig. 4*a*.

Comparison of the structures of Hjc and RuvC (5) yields less startling similarity, but nevertheless, the convex DNA-binding surface of RuvC contains basic patches surrounding the metal-binding sites. The nuclease and integrase superfamilies (RuvC is a member of the latter) do, however, share some structural homology (34) that allows an alignment of Hjc and RuvC. Both are α/β proteins, and superposition of one monomer of each produces an rms difference in C^{α} position of 2.0 Å for 27 equivalent residues, which extends to 2.2 Å for 50 residues if chain direction and sequence order are ignored. It should be noted that the location of the metal-binding site relative to the structurally conserved core is preserved (Fig. 2). The different overall topologies have been cited to discount an evolutionary connection (3, 35), but a common unit of two parallel β-strands and an α-helix (strands C, F, and helix 2 in Hjc) is conserved structurally and topologically among the fold families represented in Fig. 2, and may represent a recycled divalent metal-/phosphate-binding domain.

Given the similar functions of Hjc and RuvC, it is notable that their dimers are formed by a completely different part of the molecule, on faces 90° apart. This variance seems to translate to their differing DNA-cutting patterns. Hjc cuts at a point 3 bases 3′ to the point of strand exchange, whereas RuvC cuts exactly at the point of exchange. A feature of the type II restriction endonucleases is the variety of ways the nuclease domains are arranged to make pairwise nicks in DNA. Arrangements of the nuclease modules, such as those shown in Fig. 4*b*, illustrate the extension of this principle to the junction-resolving enzymes.

In conclusion, the structure of Hjc confirms its assignment to the nuclease superfamily of DNA restriction and repair enzymes, as predicted on the basis of limited sequence similarities. The high level of structural homology with the type II restriction endonucleases allows the identification of the active site and a proposed location for binding of the scissile duplex DNA arm of the substrate junction. Consistent with their related junction-resolving activities, striking superficial similarity to the T4 phage endonuclease VII is observed despite a total lack of structural homology. Based on a combination of the functional and structural data, we propose a mode of binding of the Holliday junction that implicates conserved residues remote from the active site.

We thank the staff at the European Synchrotron Radiation Facility (Grenoble, France), particularly Gordon Leonard, for help in data collection. This work has been funded by the Wellcome Trust and the Biotechnology and Biological Sciences Research Council. M.F.W. is a Royal Society University Research Fellow.

1. West, S. C. (1997) *Annu. Rev. Genet.* **31,** 213–244.
2. Shinagawa, H. & Iwasaki, H. (1996) *Trends Biochem. Sci.* **21,** 107–111.
3. Lilley, D. M. J. & White, M. F. (2000) *Proc. Natl. Acad. Sci. USA* **97,** 9351–9353.
4. White, M. F., Giraud-Panis, M. J., Pohler, J. R. & Lilley, D. M. J. (1997) *J. Mol. Biol.* **269,** 647–664.
5. Ariyoshi, M., Vassylyev, D. G., Iwasaki, H., Nakamura, H., Shinagawa, H. & Morikawa, K. (1994) *Cell* **78,** 1063–1072.
6. Raaijmakers, H., Vix, O., Toro, I., Golz, S., Kemper, B. & Suck, D. (1999) *EMBO J.* **18,** 1447–1458.
7. Hadden, J. M., Convery, M. A., Declais, A. C., Lilley, D. M. J. & Phillips, S. E. V. (2001) *Nat. Struct. Biol.* **8,** 62–67.
8. Woese, C. R., Kandler, O. & Wheelis, M. L. (1990) *Proc. Natl. Acad. Sci. USA* **87,** 4576–4579.
9. Komori, K., Sakae, S., Shinagawa, H., Morikawa, K. & Ishino, Y. (1999) *Proc. Natl. Acad. Sci. USA* **96,** 8873–8878.
10. Kvaratskhelia, M. & White, M. F. (2000) *J. Mol. Biol.* **297,** 923–932.
11. Kvaratskhelia, M., Wardleworth, B. N., Norman, D. G. & White, M. F. (2000) *J. Biol. Chem.* **275,** 25540–25546.
12. Kovall, R. A. & Matthews, B. W. (1999) *Curr. Opin. Chem. Biol.* **3,** 578–583.
13. Otwinowski, Z. & Minor, W. (1996) *Methods Enzymol.* **276,** 307–326.
14. Terwilliger, T. C. & Berendzen, J. (1999) *Acta Crystallogr. D* **55,** 849–861.
15. Terwilliger, T. C. (2000) *Acta Crystallogr. D* **56,** 965–972.
16. Perrakis, A., Morris, R. & Lamzin, V. S. (1999) *Nat. Struct. Biol.* **6,** 458–463.
17. Jones, T. A., Zou, J. Y., Cowan, S. W. & Kjeldgaard, M. (1991) *Acta Crystallogr. A* **47,** 110–119.
18. Collaborative Computational Project Number 4. (1994) *Acta Crystallogr. D* **50,** 760–764.
19. Kleywegt, G. J. & Brunger, A. T. (1996) *Structure (London)* **4,** 897–904.
20. Laskowski, R. A., MacArthur, M. W., Moss, D. S. & Thornton, J. M. (1993) *J. Appl. Crystallogr.* **26,** 283–291.
21. Hooft, R. W., Vriend, G., Sander, C. & Abola, E. E. (1996) *Nature (London)* **381,** 272.
22. Holm, L. & Sander, C. (1995) *Trends Biochem. Sci.* **20,** 478–480.
23. Daiyasu, H., Komori, K., Sakae, S., Ishino, Y. & Toh, H. (2000) *Nucleic Acids Res.* **28,** 4540–4543.
24. Baldwin, G. S., Sessions, R. B., Erskine, S. G. & Halford, S. E. (1999) *J. Mol. Biol.* **288,** 87–103.
25. Vipond, I. B., Baldwin, G. S. & Halford, S. E. (1995) *Biochemistry* **34,** 697–704.
26. Komori, K., Sakae, S., Daiyasu, H., Toh, H., Morikawa, K., Shinagawa, H. & Ishino, Y. (2000) *J. Biol. Chem.* **275,** 40385–40391.
27. Komori, K., Sakae, S., Fujikane, R., Morikawa, K., Shinagawa, H. & Ishino, Y. (2000) *Nucleic Acids Res.* **28,** 4544–4551.
28. Kleywegt, G. J. & Jones, T. A. (1997) *Methods Enzymol.* **277,** 525–545.
29. Kostrewa, D. & Winkler, F. K. (1995) *Biochemistry* **34,** 683–696.
30. Deibert, M., Grazulis, S., Janulaitis, A., Siksnys, V. & Huber, R. (1999) *EMBO J.* **18,** 5805–5816.
31. Athanasiadis, A., Vlassi, M., Kotsifaki, D., Tucker, P. A., Wilson, K. S. & Kokkinidis, M. (1994) *Nat. Struct. Biol.* **1,** 469–475.
32. Usher, K. C., de la Cruz, A. F., Dahlquist, F. W., Swanson, R. V., Simon, M. I. & Remington, S. J. (1998) *Protein Sci.* **7,** 403–412.
33. Rafferty, J. B., Sedelnikova, S. E., Hargreaves, D., Artymiuk, P. J., Baker, P. J., Sharples, G. J., Mahdi, A. A., Lloyd, R. G. & Rice, D. W. (1996) *Science* **274,** 415–421.
34. Venclovas, C. & Siksnys, V. (1995) *Nat. Struct. Biol.* **2,** 838–841.
35. Yang, W. & Steitz, T. A. (1995) *Structure (London)* **3,** 131–134.
36. Kraulis, P. J. (1991) *J. Appl. Crystallogr.* **24,** 946–950.
37. Merritt, E. A. & Bacon, D. J. (1997) *Methods Enzymol.* **277,** 505–524.
38. Barton, G. J. (1993) *Protein Eng.* **6,** 37–40.
39. Kabsch, W. & Sander, C. (1983) *Biopolymers* **22,** 2577–2637.
40. Hutchinson, E. G. & Thornton, J. M. (1996) *Protein Sci.* **5,** 212–220.
41. Nicholls, A., Bharadwaj, R. & Honig, B. (1993) *Biophys. J.* **64,** 166–170.